Available online at www.sciencedirect.com
SCIENCE DIRECT
Journal of Molecular Catalysis A: Chemical 245 (2006) 78–86
JOURNAL OF MOLECULAR CATALYSIS A: CHEMICAL
www.elsevier.com/locate/molcata

Photoassisted fenton degradation of nonbiodegradable azo-dye (Reactive Black 5) over a novel supported iron oxide catalyst at neutral pH

Chan-Li Hsueh [a], Yao-Hui Huang [a], Cheng-Chien Wang [b], Chuh-Yung Chen [a,*]

[a] *Department of Chemical Engineering, National Cheng Kung University, Tainan City 701, Taiwan*
[b] *Department of Chemical Engineering, Southern Taiwan University of Technology, Tainan City 710, Taiwan*

Received 18 March 2005; received in revised form 19 September 2005; accepted 29 September 2005
Available online 25 October 2005

Abstract

A novel supported iron oxide, prepared using a fluidized-bed reactor (FBR), was utilized as a catalyst of the heterogeneous photoassisted Fenton degradation of azo-dye Reactive Black 5 (RB5). This catalyst is much cheaper than Nafion-based catalysts, and can markedly accelerate the degradation of RB5 under irradiation by UVA ($\lambda = 365$ nm). The effects of the molar concentration of H_2O_2, the pH of the solution and the catalyst loading on the degradation of RB5 are elucidated. A simplified mechanism of RB5 decomposition that is consistent with the experimental findings for a solution with a pH of up to 7.0 is proposed. About 70% decolorization was measured and 45% of the total organic carbon was eliminated on the surface of the iron oxide at pH 7.0 after 480 min in the presence of 0.055 mM RB5, 5.0 g iron oxide/L, 29.4 mM H_2O_2, under 15 W UVA.

Keywords: Iron oxide; Reactive Black 5; Decolorization; Mineralization

1. Introduction

Reactive Black 5 is one of the oldest reactive dyes and is consumed very heavily in textile dyeing [1]. Environmentally, the removal of synthetic dyes is of particular concern, because they, or their degradation products, may be toxic so their treatment cannot depend on biodegradation alone. Accordingly, the degradation of dyehouse effluents has become a critical step in treating textile wastewater [1].

In the last decade, Fenton and photoassisted Fenton reactions have been extensively utilized to degrade aromatic organic compounds in industrial wastewater. Their effectiveness follows from high reactivity and nonselectivity of the generated hydroxyl radicals ($OH^{\bullet}$), which can therefore decompose numerous organic compounds [2–11]. Notably, however, the large volume of the Fe(III)-iron sludge following a Fenton reaction is a serious problem because removing Fe(III)-iron sludge at the end of treatment by precipitation is rather expensive.

The authors previously studied [12–14] the FBR–Fenton process, in which a fluidized bed is used to transform Fe(III), generated in Fenton's reaction, into an iron oxide (such as FeOOH) on the carrier surface by crystallization or sedimentation, to eliminate this obvious problem described above [12]. The FBR–Fenton process combines the functions of homogeneous chemical oxidation (H_2O_2/Fe^{2+}), heterogeneous chemical oxidation (H_2O_2/FeOOH), fluidized bed crystallization and the reductive dissolution of FeOOH. This process not only provides a high COD removal efficiency but also reduces the large amount of Fe sludge produced [13]. Moreover, the FeOOH synthesized in the reaction between H_2O_2 and Fe^{2+} also acts as a heterogeneous catalyst of the decomposition H_2O_2 [14]. Some full-scale FBR–Fenton reactors have been constructed to treat bioeffluent from industrial wastewater in Taiwan.

Efforts have recently been made to develop a heterogeneous photoassisted Fenton reaction [15–22]. For example, Fernandez et al. [15,16] successfully prepared an Fe^{3+}/Nafion membrane catalyst using a simple ion exchange reaction and utilized it in the photoassisted Fenton degradation of an azo-dye Orange II. Puma and Yue [22] investigated the photoassisted Fenton reaction of indigo carmine dye on an Fe/Nafion pellet and determined that the catalyst very effectively reduces the concentration of indigo carmine dye. However, the Nafion film or pellet-based catalysts have two major shortcomings that considerably constrain their practical usefulness on a large scale. The first is their

* Corresponding author. Tel.: +886 6 2757575 62643; fax: +886 6 2344496.
E-mail address: ccy7@ccmail.ncku.edu.tw (C.-Y. Chen).

1381-1169/$ – see front matter © 2005 Elsevier B.V. All rights reserved.
doi:10.1016/j.molcata.2005.09.044

weak photocatalytic activity associated with their low surface area. The second is that the Nafion film is too expensive for practical use. Therefore, Feng et al. [20,21] used Laponite RD instead of Nafion film. A search on the Internet revealed that the price of Nafion exceeds 2000 US$/kg while that of Laponite RD is less than 40 US$/kg [20,21]. Hence, much cheaper heterogeneous catalysts of the photoassisted Fenton reaction must be found. This study explores an iron oxide material, which is a by-product of the FBR–Fenton reaction, for use in the treatment of the bioeffluent of tannery wastewater from a dyeing/finishing plant in Taiwan. The goal of this study is to elucidate the heterogeneous photoassisted Fenton degradation of RB5 using iron oxide obtained from an FBR–Fenton reactor as a heterogeneous catalyst. The effects of some important variables on the degradation of RB5 are investigated in detail. This investigation is more concerned about recycling iron oxide for treating wastewater using the photoassisted Fenton process, than it is with the kinetics or the reaction path. Although identifying intermediates during the degradation of RB5 is very important, this study considers more closely the extent of mineralization of RB5 in the presence of iron oxide, H_2O_2 and UVA light, because the authors believe that in real industrial applications, total organic carbon (TOC) removal is more important than identifying the intermediates. If the TOC can be removed, then the intermediate organics have been oxidized to water and carbon dioxide. Furthermore, iron oxide and hydrogen peroxide are common constituents of natural and atmospheric water [23]. Hence, studying the photoreaction in the iron oxide/H_2O_2/organics system under UVA irradiation improves our understanding of the mechanism of photo-oxidation in the environment.

2. Experimental

2.1. Materials

RB5, $C_{26}H_{21}N_5Na_4O_{19}S_6$, was purchased from Aldrich Chemical company (Amherst, NY, USA); it was 55% pure, and had a molecular weight of 991.82. The structure of RB5 is presented below. $NaClO_4$ (Merck) and H_2O_2 (Union Chemical) were of analytical reagent grade and were used without further purification. Activated alumina grain was obtained from Alcoa Chemicals. Deionized and doubly distilled water were used throughout this investigation.

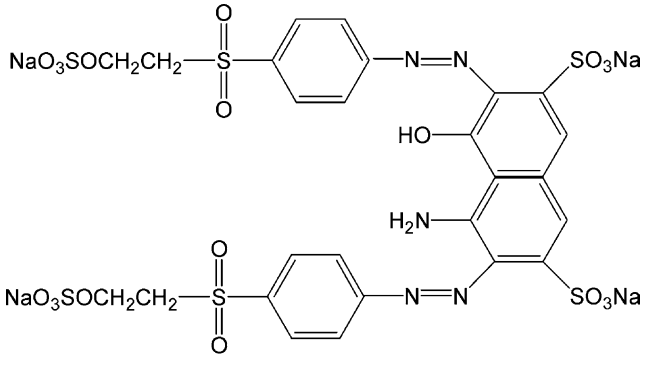

Reactive Black 5 (RB5)

2.2. Catalyst preparation

A novel catalyst, iron oxide on a activated alumina support, was prepared in the following manner [24]. Activated alumina grains were packed in a 30 m^3 FBR (2.1 m Ø × 9 m height). The internal circulation of the FBR was controlled to maintain an up flow superficial velocity of 40 m h^{-1} with a 50% bed expansion. The bioeffluents of tannery wastewater, H_2O_2 and $FeSO_4$ were fed continuously into the reactor bottom. The molar ratio of H_2O_2 to $FeSO_4$ was 2:1. The pH of the solution, which was adjusted by adding dilute aqueous solutions of NaOH or H_2SO_4, was maintained at 3, to prevent the precipitation of $Fe(OH)_3$ [25]. After the reaction had proceeded for around three months, iron oxide was coated onto the surface of the activated alumina grains to enable catalytic oxidation.

The iron oxide was identified from the nitrogen adsorption data obtained at the temperature of liquid nitrogen using an automated adsorption instrument (Micromeritics ASAP 2010, USA). The Brunauer–Emmett–Teller (BET) surface area and porosity of the catalyst were obtained from the data of the isotherms. The surface area of the catalyst was calculated using the BET equation.

Morphology of the activated alumina grain support and catalyst were determined using a Hitachi S-400 scanning electron microscope (SEM). The atomic composition of the iron oxide surface was elucidated by energy dispersive spectra (EDS) using an Oxford INCA-400 spectrometer. Intrinsic acidity constants (K_{a1} and K_{a2}) were obtained from graphic extrapolation of transformed acid/base titration data to zero surface charge conditions [26].

Anion analysis was conducted using a Mertohm model 733 ion chromatograph (IC) equipped with an Metrosep A Supp 4/5 Guard column (Mertohm) and operating in the suppressed conductivity detention mode. Sample injected by an automatic sampler, were eluted by a $NaHCO_3/Na_2CO_3$/water gradient at a flow rate of 0.8 ml/min.

2.3. Methods and apparatus

The photocatalytic activity of the iron oxide in degrading the RB5 solution in a batch photoreactor (Fig. 1) at room temperature was evaluated under illumination at intensity of 1.8 mW cm^{-2}. The irradiation source was a 15 W UVA lamp (UVP BL-15 365 nm) fixed inside a cylindrical Pyrex tube (allowing wavelengths $\lambda > 320$ nm to pass). This setup prevented the formation of $OH^{\bullet}$ radicals by the direct photolysis of H_2O_2. The total volume of the solution was 1200 mL; the initial concentration of RB5 was 0.055 mM. Specified amounts of $NaClO_4$ and H_2O_2 were dripped into the reactor. The pH of the solution was controlled at 7.0 (except where otherwise specified) using a pH meter (Action, A211). The pH of the solution was altered by adding diluted aqueous solutions of NaOH or $HClO_4$. The starting point of the reaction was defined as the time when the UVA light was turned on and a certain quantity of iron oxide was added to the photoreactor. Compressed air was bubbled from the bottom at a flow rate of about 1800 mL/min and it was exposed to the ambient air effectively to suspend the catalyst in

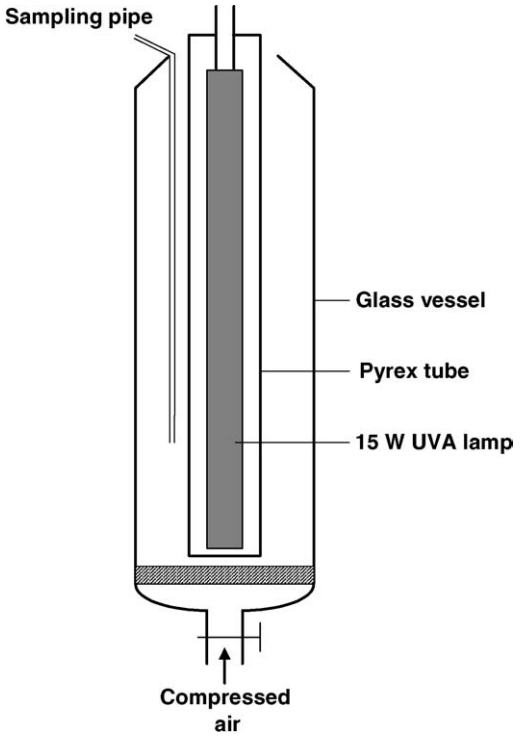

Fig. 1. Schematic diagram of the photoreactor apparatus.

the reactor and ensure good mixing. Samples were periodically extracted from the reactor using a pipe, and were immediately analyzed using a UV–vis spectrometer after they had been filtered through a 0.25 μm syringe filter made of poly-(vinylidene fluoride) to remove iron oxide particles.

The RB5 spectrum showed an absorption peak at 597 nm. Therefore, the concentration of RB5 solution was determined from the absorption intensity at 597 nm using a UV–vis spectrometer (Jasco Model 7850). Before the measurement was made, a calibration curve was plotted using the standard RB5 with known concentrations. The residual H_2O_2 was determined photometrically using potassium titanium oxalate in mineral acid [27]. In addition, an atomic absorbance spectrophotometer (GBC Avanta) was used for dissolved iron determination in solution. TOC was analyzed using a Shimadzu 500 TOC analyzer.

3. Results and discussion

3.1. Characterization of the catalyst

Fig. 2 presents SEM micrographs of the activated alumina grain support, and the iron oxide prepared through a FBR. Fig. 2a (100×) and b (300×) indicate that the original activated alumina grain support is irregularly shaped. It was smoother after the reaction in the FBR had proceeded for 3 months, as displayed in Fig. 2c (100×) and d (300×). The cation-exchange capacities (CEC) of the original activated alumina grain support and the iron oxide are 0.39 and 0.47 mequiv. g^{-1}, respectively. Table 1 lists the other properties of the iron oxide.

Table 1
Properties of the iron oxide

Parameter	Value
Total Iron content of catalyst (g kg^{-1})	304
Bulk density (g cm^{-3})	1.43
Absolute (true) density (g cm^{-3})	2.66
Specific surface area (m^2 g^{-1})	170
Total pore volume (cm^3 g^{-1})	0.12
Cation-exchange capacities (mequiv. g^{-1})	0.47
pK_{a1}	6.03
pK_{a1}	8.67
pH_{pzc} (point of zero charge)[a]	7.35

[a] $pH_{pzc} = (pK_{a1} + pK_{a2})/2$.

Fig. 3 displays the EDS of the activated alumina grain support (curve a) and iron oxide (curves b). Curve a indicates that O and Al are the dominant elements detected on the surface of the activated alumina grain support. However, curve b reveals that Fe and C are added to the surface of iron oxide after three months of reaction in the FBR. Table 2 presents the quantitative surface chemical compositions of the iron oxide, determined by EDS. In a previous study [13], the main constituent on the surface of the catalyst was identified as γ-FeOOH. The presence of C in the iron oxide stimulated the authors' interest. Hence, 5 g iron oxide was put into 100 ml of 1 M hydrochloric acid for 24 h to dissolve the iron oxide. Thereafter, the pH of the solution was adjusted to 2.5 by NaOH and filtered using a 0.25 μm poly-(vinylidene fluoride) filter. Finally, the sample solution was analyzed using an ion chromatograph. Fig. 4 reveals that oxalate (indicated by the arrow in Fig. 4) is detected by comparison with an authentic standard. Several investigations [28–30] have revealed that oxalates were obtained by the oxidation of the dyes. The catalyst was a by-product of the FBR–Fenton reaction for treating dyeing/finishing plant, which fact perhaps explains why oxalate is present in the bulk phase of the catalysts. However, whether the presence of oxalate in the iron oxide is caused by adsorption or is a formed structure similar to that of Fe(III)–oxalate complexes [31], cannot presently be explained. Moreover, Fig. 4 includes some unknown peaks. This will be a subject of our future works.

Fig. 5 depicts the quantity of RB5 adsorbed onto the catalyst at various pH values of the solution in two days in a jar test. The initial concentration of RB5 ($C_{RB5,0}$) was 0.055 mM. The figure indicates that those in acid and neutral solutions adsorbed more RB5 than those in alkaline solutions. The marked difference between the adsorptions at pH 7 and 8 is explained by the characteristics of the iron oxide. The pH value of zero charge (pH_{pzc}) of the iron oxide is approximately 7.35 (Table 1); the surface is positively charged at a lower pH. This favors the adsorption

Table 2
Surface atomic compositions and binding energy (BE) of support (activated alumina grain) and iron oxide by EDS

Element	Support (at.%)	Iron oxide (at.%)	Binding energy (keV)
Al	47.62	0.95	0.277
O	52.38	48.87	0.525
C	0	10.51	1.487
Fe	0	39.67	0.628, 0.705, 6.404, 7.058

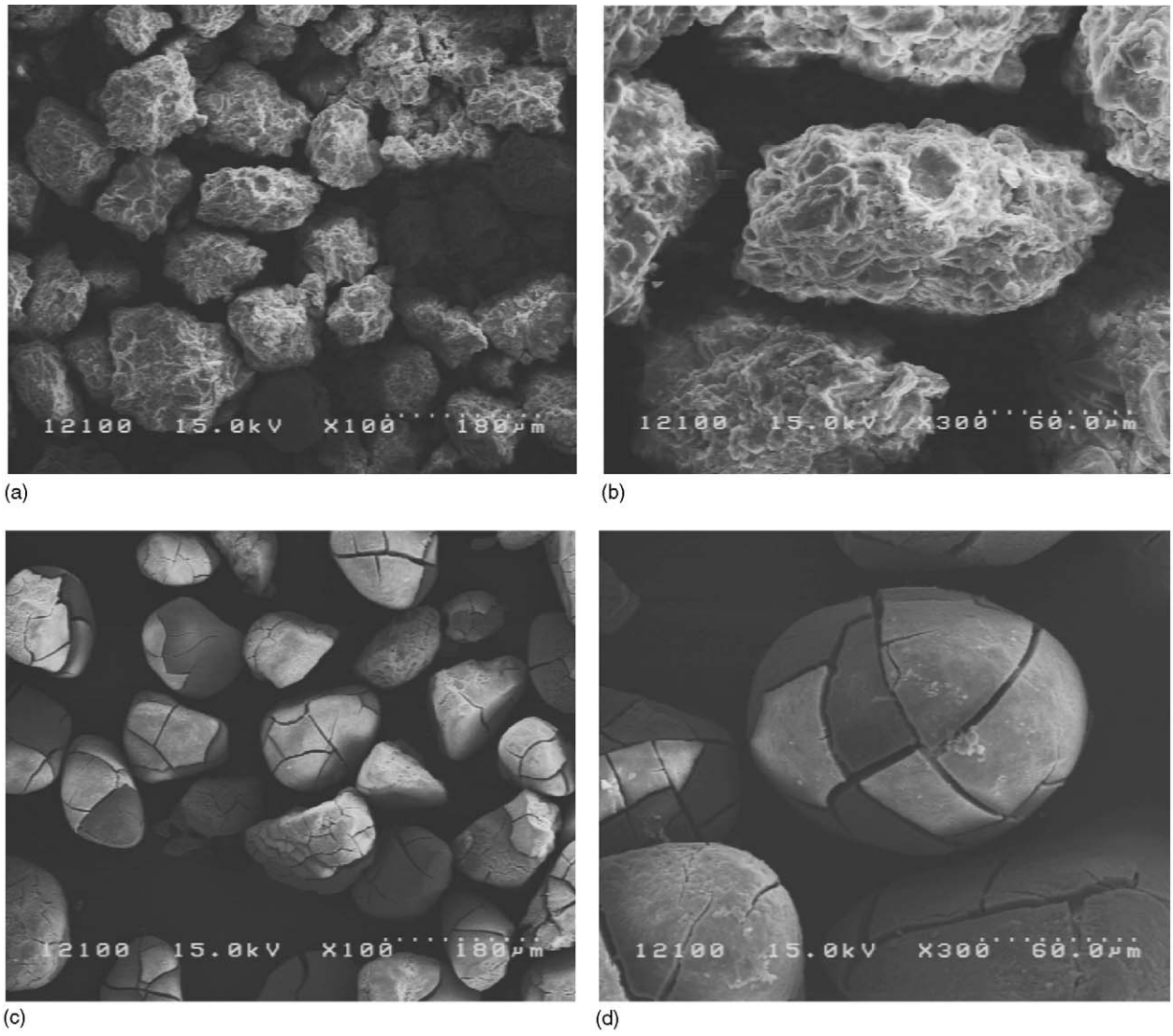

Fig. 2. Scanning electron micrographs of original activated alumina grain support: (a) 100×; (b) 300× and iron oxide: (c) 100×; (d) 300×.

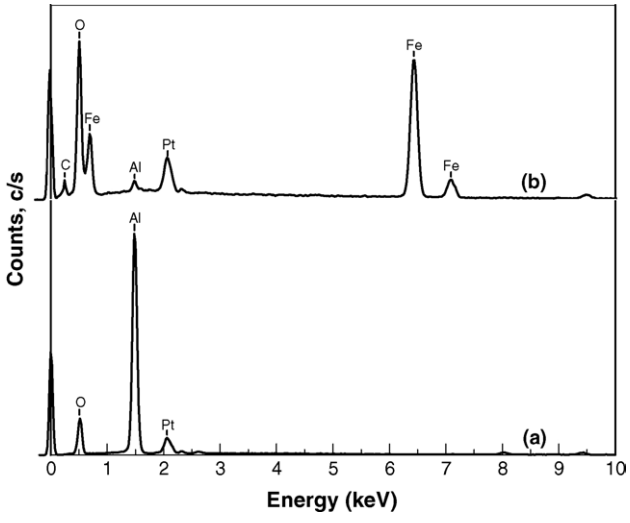

Fig. 3. EDS spectra of (a) original activated alumina grain support and (b) iron oxide.

of the anionic dye RB5. The surface is negatively charged at a higher pH value (>7.35), disfavoring adsorption of the anionic dye RB5. At pH 12.0, the amount of RB5 adsorbed onto the catalyst during the first 4 h was almost zero. Hence, the RB5 adsorbed in acid and neutral solutions was desorbed from the catalyst by adjusting the solution to pH 12.0. The results demonstrate that over 95% RB5 can be desorbed in 10 min at pH 12.0.

3.2. Degradation of Reactive Black 5

The photocatalytic activity of the catalyst in the degradation of 0.055 mM RB5 was evaluated under UV irradiation with a wavelength of 365 nm at pH 7.0. Fig. 6A plots the RB5 concentration against reaction time (0–240 min) under various conditions. Without H_2O_2 or a catalyst, but with only 15 W UVA (curve a), the RB5 concentration hardly declined, indicating that the degradation of RB5 by photolysis is very weak. Without H_2O_2 and 15 W UVA, and with only 5.0 g of catalyst/L (curve b), the RB5 concentration dropped by around 50% dur-

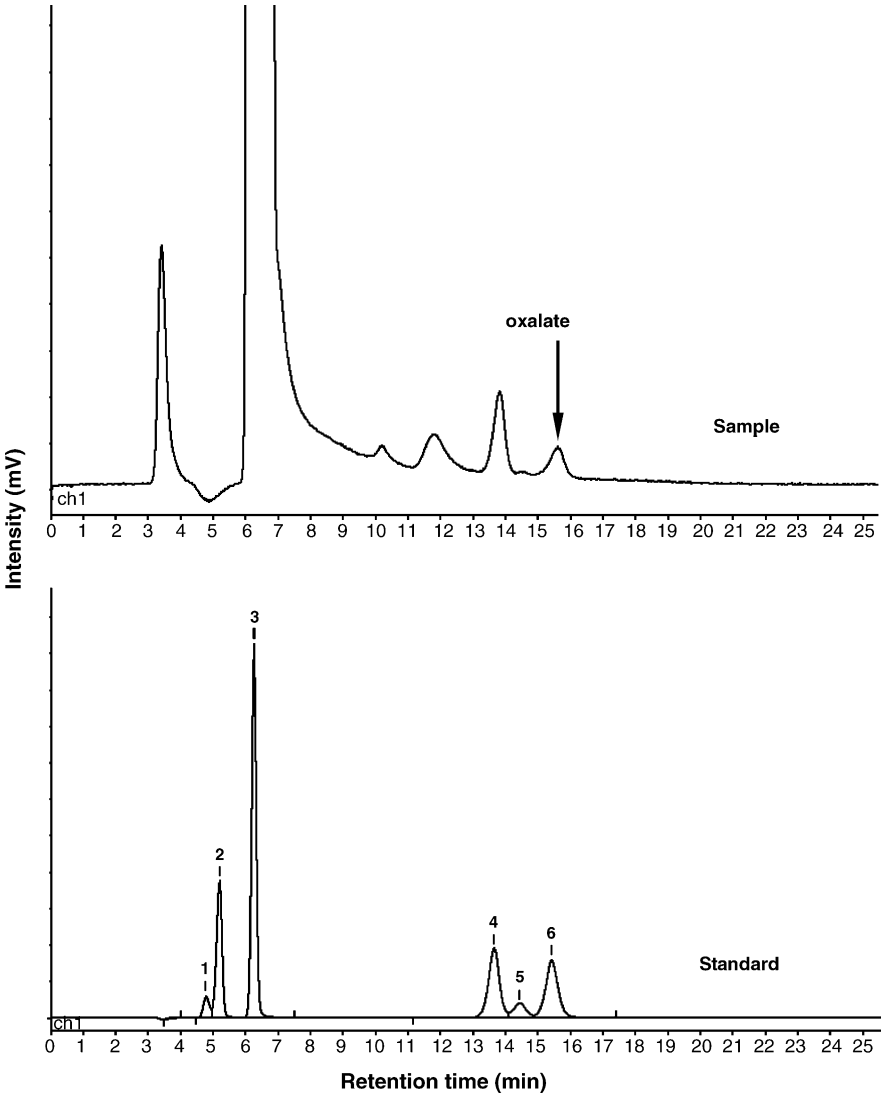

Fig. 4. Detection of solution of iron oxide in hydrochloric acid by ion chromatograph. Standard peak identities are as follows: (1) formate; (2) acetata; (3) chloride; (4) sulfate; (5) succinate; (6) oxalate.

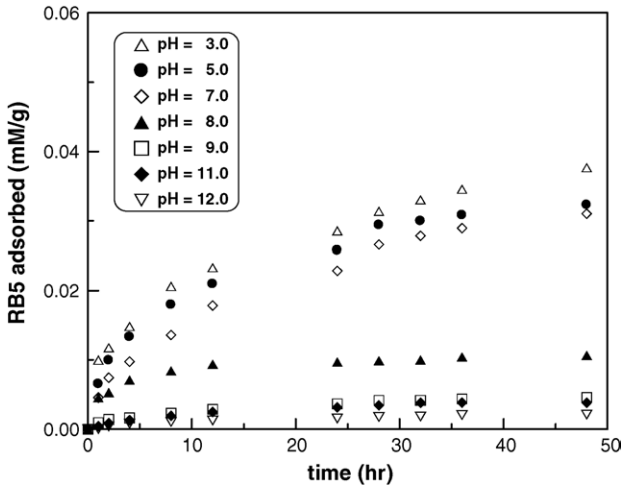

Fig. 5. Effect of the solution pH on the adsorption data of 0.055 mM RB5 under 1.0 g iron oxide/L, 5.0 mM $NaClO_4$, 30 °C.

ing 240 min of reaction. When the solution pH was adjusted to 12.0, the RB5 concentration in the solution returned to 95.2% of the initial RB5 concentration in 10 min revealing physical adsorption and desorption between RB5 and the catalyst.

Without a catalyst but with 29.4 mM H_2O_2 and 15 W UVA (curve c in Fig. 6A), the degradation of RB5 is very limited (<10%) after 240 min of reaction. Oxidation by $OH^{\bullet}$ radicals, which were generated by the direct photolysis of H_2O_2 under UVA may have been responsible for the decrease in the concentration of RB5. Without 15 W UVA but with 29.4 mM H_2O_2 and 5.0 g catalyst/L in the dark (curve d), the RB5 concentration decreases rapidly initially and then decreases more slowly, perhaps because of the combined effect of adsorption and the Fenton-like reaction at the surface of the catalyst. RB5 is firstly adsorbed onto the surface of the catalyst and then oxidized by the Fenton-like reaction. After some of the intermediates have redissolved from the catalyst surface into the solution, the residual RB5 is continuously adsorbed and oxidized. The degradation of

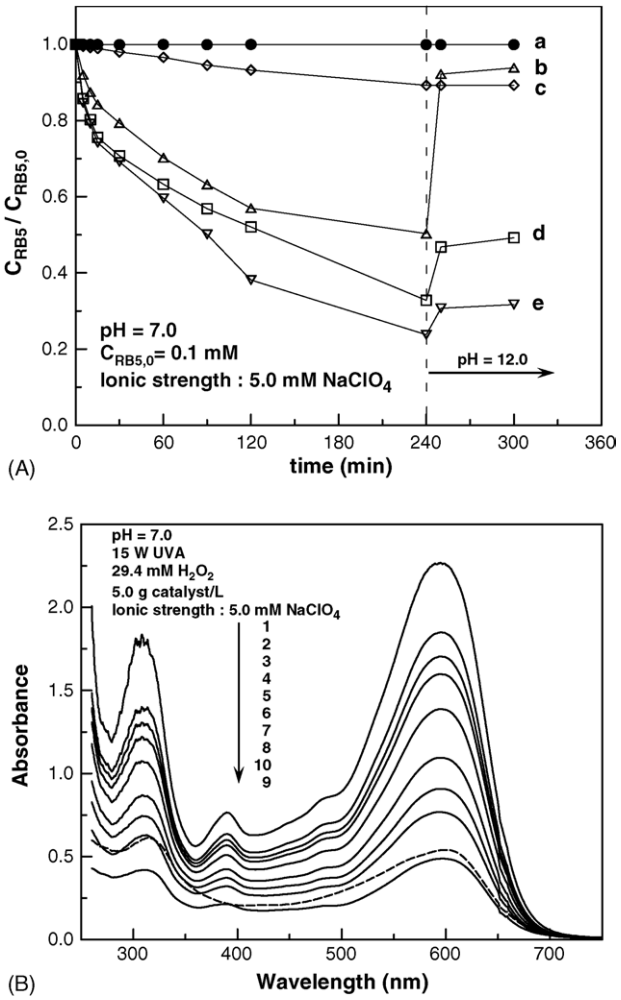

Fig. 6. (A) RB5 concentration vs. the reaction time under various conditions: (a) without H_2O_2 and iron oxide but with 15 W UVA; (b) without H_2O_2 but with 5.0 g of catalyst/L and 15 W UVA; (c) without iron oxide but with 29.4 mM H_2O_2 and 15 W UVA; (d) in the dark but with 29.4 mM H_2O_2 and 5.0 g of catalyst/L; (e) with 29.4 mM H_2O_2, 5.0 g of catalyst/L, and 15 W UVA. (B) UV–vis adsorption spectral changes of the RB5 (0.055 mM) solution in H_2O_2 (29.4 mM)/iron oxide (5 g L^{-1}) dispersion under 15 W UVA irradiation; spectra 1–9 denote the reaction time 0, 5, 10, 15, 30, 60, 90, 120, and 240 min at pH 7.0, respectively; spectra 10 denotes the time 300 min at pH 12.0 (desorption).

RB5 is most rapid in the presence of 5.0 g catalyst/L, 29.4 mM H_2O_2 and 15 W UVA (curve e in Fig. 6A). The formation of Fe(II) by light on the surface of the catalyst generates $OH^{\bullet}$ radicals by decomposing H_2O_2, promoting the degradation of RB5 [16].

Fig. 6B presents the changes in UV–vis spectra during the degradation of RB5 in the presence of the catalyst and H_2O_2 under UVA light irradiation at pH 7.0 (spectra 1–9). RB5 exhibits absorption bands at 597, 391 and 313 nm. The absorption peaks dropped under UVA light irradiation. The visible and ultraviolet regions exhibited no new absorption band, revealing that the conjugated structure was destroyed [32]. Fig. 6B also shows the spectrum obtained following desorption (spectrum 10). A careful comparison between spectrum 9 and 10 clearly shows that the two clearly differ. Firstly, the absorption peak at 391 nm disappeared because RB5 exhibits no peak there at pH 12. Secondly,

Table 3
The comparison of absorbent data between Fig. 6B and RB5

	λ (nm)	313	597
RB5			
	Absorbance at pH 12	0.907	1.273
	Absorbance at pH 7	0.818	1.275
	Ratio of absorbance $\frac{\text{pH 12}}{\text{pH 7}}$	1.11	0.998
Fig. 6B			
	Absorbance of spectrum 10	0.613	0.54
	Absorbance of spectrum 9	0.418	0.488
	Ratio of absorbance $\frac{\text{spectrum 10}}{\text{spectrum 9}}$	1.47	1.11
	$\frac{\text{spectrum 10/spectrum 9}}{\text{pH 12/pH 7}}$	1.32	1.11

Table 3 indicates that the rise in the intensity of the absorption band at 313 nm after desorption exceeds that at 597 nm, revealing that the adsorption of intermediates, which were desorbed from the surface of the catalyst into the solution, was responsible for the difference between spectrum 9 and 10.

3.3. Effect of H_2O_2 molar concentration

In a Fenton or photoassisted Fenton reaction, the molar concentration of H_2O_2 critically affects the degradation of organic compounds because the H_2O_2 molar concentration is directly related to the number of $OH^{\bullet}$ radicals produced in the Fenton or photoassisted Fenton reaction. The degradation rate of organic compounds usually rises with the concentration until a critical concentration is reached. When the concentration is higher than the critical concentration, the so-called scavenging effect reduces the degradation rate of organic compounds. Numerous groups have observed this phenomenon [18,20].

Fig. 7 plots the RB5 concentration against reaction time (0–240 min) for various molar concentrations of H_2O_2. During the first 60 min, the degradation of RB5 is greatly enhanced as the molar concentration increases from 0 to 29.4 mM, because more $OH^{\bullet}$ radicals are formed at higher H_2O_2 molar concentrations in solution. However, when the H_2O_2 molar concentration

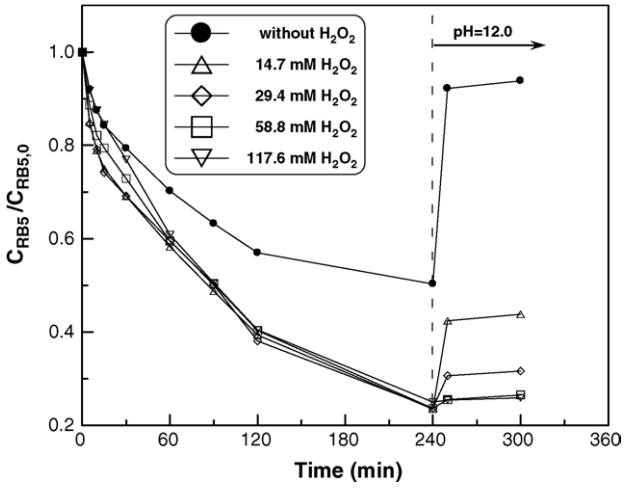

Fig. 7. Effect of the H_2O_2 molar concentration on the degradation of 0.055 mM RB5 accompanied with simultaneous decomposition of H_2O_2 under 5.0 g catalyst/L, 15 W UVA, pH 7.0, 5.0 mM $NaClO_4$.

exceeds 29.4 mM, the degradation of RB5 slightly slows down. This result is explained by the so-called scavenging effect on the further generation of $OH^{\bullet}$ radicals on the surface of catalyst when a higher molar concentration of H_2O_2 is employed, as described by the following equation [16,33]:

$$H_2O_2 + OH^{\bullet} \rightarrow HO_2^{\bullet} + H_2O \quad (1)$$

The degradations of RB5 at various H_2O_2 concentrations are very close at reaction times between 60 and 240 min. This result indicates that, although the oxidative ability of $OOH^{\bullet}$ radicals is weaker than $OH^{\bullet}$ radicals, such $OOH^{\bullet}$ radicals can also attack and remove RB5 when a high molar concentration of H_2O_2 is used.

Following desorption at pH 12, the concentration of RB5 varies interestingly. Apparently, as the H_2O_2 molar concentration increases from 0 to 58.8 mM, the concentration of desorbed RB5 decreases, but the RB5 desorbed by 29.4 mM H_2O_2 differs by only 5% from that desorbed by 58.8 mM H_2O_2. When the H_2O_2 molar concentration exceeds 58.8 mM, the desorbed RB5 no longer increases.

The above results and a consideration of the costs of industrial applications in the future indicate that a suitable H_2O_2 molar concentration for degrading 0.055 mM RB5 is around 29.4 mM.

3.4. Effect of the catalyst loading

Catalyst loading is an important factor that can substantially affect the photoassisted Fenton reaction. Higher catalyst loading leads to more rapid degradation of organic compounds.

Fig. 8 plots the RB5 and H_2O_2 concentrations against reaction time (0–240 min) for various loadings of the catalyst. Changing the catalyst loading from 1 to 5.0 g catalyst/L substantially promotes the degradation of RB5. Additionally, the decomposition rate of H_2O_2 increased with the catalyst loading. The amount of residual H_2O_2 was very close to zero following 240 min of reaction, when 5.0 g catalyst/L was used. These results indicate that an appropriate catalyst loading was 5.0 g catalyst/L, which was used in the remaining experiments.

3.5. Effect of the solution pH

RB5 was photdegraded at pH values from 5 to 9 in the catalyst/H_2O_2 system (Fig. 9). Clearly, the reaction occurred over a wide range of pH values from acidic to alkaline, unlike in the Fenton system (pH ≈ 3). Fig. 9 reveals that the degradation rate decreases as the initial solution pH increases. No free Fe ions were detected during the reaction by atomic absorbance spectrophotometry in any case. This finding supports the adsorption data. Fig. 5 indicates that the catalyst adsorbs more RB5 in acidic or neutral media (pH 5.0 or 7.0) than in alkaline solutions (pH 9.0). Accordingly, the degradation of RB5 at pH 5.0 and 7.0 is more rapid than at pH 9.0. RB5 was completely removed from the bulk solution at pH 5.0 and approximately 93% was removed from the surface of the catalyst. The pH of natural water is generally between 5 and 9. This study will also elucidate the role of a catalyst in the natural environment.

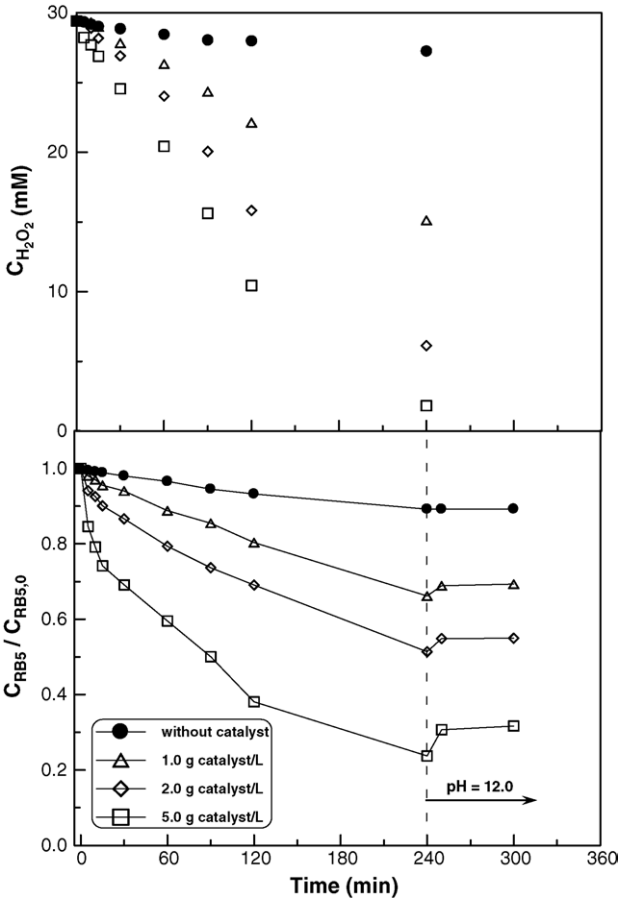

Fig. 8. Effect of the catalyst loading on the degradation of 0.055 mM RB5 accompanied with simultaneous decomposition of H_2O_2 under 29.4 mM H_2O_2, 15 W UVA, pH 7.0, 5.0 mM $NaClO_4$.

3.6. Mineralization of RB5

Reaction intermediates are known sometimes to be formed by the oxidation of organic dyes and some may be longer-lived and even more toxic to aquatic animals and human beings than

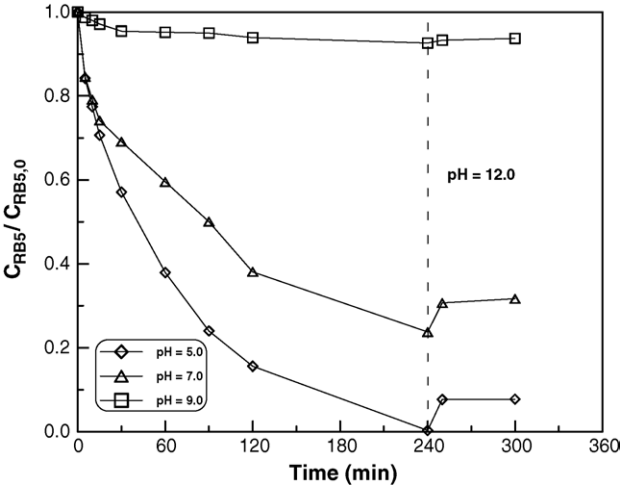

Fig. 9. Effect of the solution pH on the degradation of 0.055 mM RB5 under 29.4 mM H_2O_2, 5.0 g catalyst/L, 15 W UVA, 5.0 mM $NaClO_4$.

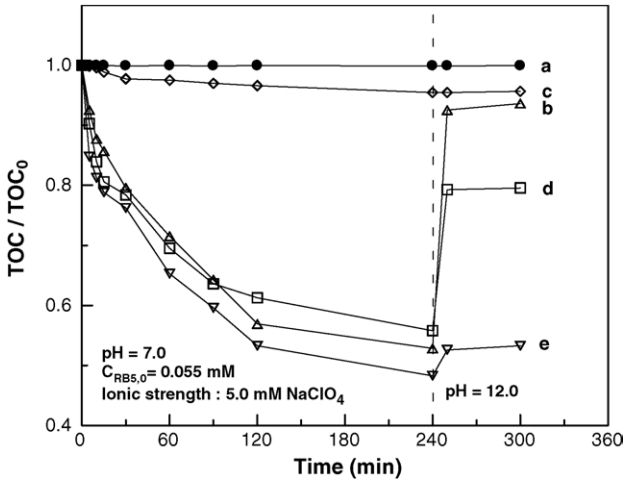

Fig. 10. TOC vs. time under different conditions: (a) without H_2O_2 and iron oxide but with 15 W UVA; (b) without H_2O_2 but with 5.0 g of catalyst/L and 15 W UVA; (c) without catalyst but with 29.4 mM H_2O_2 and 15 W UVA; (d) in the dark but with 29.4 mM H_2O_2 and 5.0 g of catalyst/L; (e) with 29.4 mM H_2O_2, 5.0 g of catalyst/L, and 15 W UVA.

parent compounds. Although identifying the intermediates is very important in determining the reaction path of the photoassisted Fenton degradation of RB5, this investigation more strongly focuses on the extent of mineralization of RB5 with reference to practical industrial applications. Although alternative techniques for evaluating the extent of mineralization of organic pollutants may be available, the removal of TOC is commonly used in the industrial treatment of wastewater to determine this extent of mineralization. Therefore, this study addresses the removal of TOC from RB5 solution, rather than on identifying reaction intermediates.

Fig. 10 plots the TOC of 0.055 mM RB5 against time (0–240 min) under various conditions. Without the catalyst or H_2O_2 but with only 15 W UVA (curve a), the TOC of RB5 does not decrease at all, revealing that the direct photolysis of RB5 cannot mineralize RB5.

With 5.0 g of catalyst/L and 15 W UVA (curve b), the TOC decreases rapidly in the first 120 min after which it decreases more slowly. Desorption considerably increases the amount of TOC in solution. As discussed earlier, the adsorption of RB5 on the surface of the catalyst is primarily responsible for this phenomenon.

With 29.4 mM H_2O_2 and 15 W UVA (curve c), only around 5% of TOC was removed in 240 min of reaction, revealing that using only H_2O_2 and 15 W UVA cannot effectively mineralize RB5. Without UVA light (in the dark), but with 29.4 mM H_2O_2 and 5.0 g of catalyst/L (curve d), the TOC decreases in the first 240 min because of both the adsorption and the oxidation of RB5 on the surface of the catalyst. Between 90 and 240 min, the TOC associated with curve d exceeds that associated with curve b, perhaps because some of the colorless intermediates redissolve into the bulk solution. Curve d indicates that following desorption, only around 20% TOC is removed and the decolorization is 50% (curve d in Fig. 6A) revealing that the $OOH^{\bullet}$ radicals can be generated in a Fenton-like reaction on the catalyst surface [34]. The $OOH^{\bullet}$ radicals can only oxidize the RB5 into

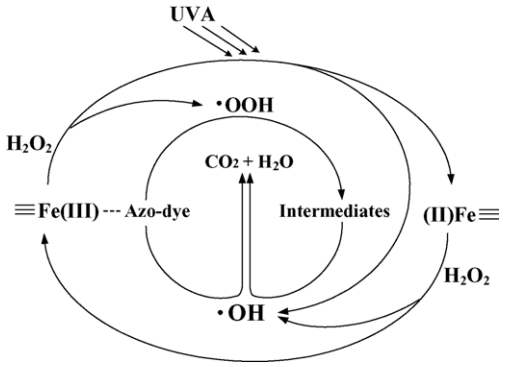

Scheme 1. Proposed mechanism for the photodegradation of azo-dye RB5 over iron oxide in the presence of H_2O_2 under UVA light irradiation.

intermediates but cannot effectively mineralize RB5 into H_2O and CO_2. Our recent investigation presented a similar finding [35].

With 29.4 mM H_2O_2, 5.0 g of catalyst/L and 15 W UVA (curve e), the TOC decreases during the first 15 min, in a manner similar to that showed associated with by curve d. As discussed above, this phenomenon is caused by both the adsorption and the Fenton-like reaction of RB5 on the surface of the catalyst. Between 15 and 240 min, the decrease in TOC indicated as curve e clearly differs from that plotted as curve d revealing that Fe(II) species are generated by UVA light on the surface of the catalyst, and that these generate $OH^{\bullet}$ radicals by the decomposition of H_2O_2 [16,31]. Curves e (light) and d (dark) indicate that about 45% and 20% TOC, respectively, are removed after 4 h of the reaction. This result clearly reveals that the presence of UVA light effectively promotes the mineralization of RB5.

3.7. Mechanism for catalyst as a heterogeneous photoassisted fenton reaction

Based on the above results, the following simple mechanism for this system is presented as Scheme 1.

Fe(III) initiates the reaction on the surface of the catalyst (≡Fe(III)), accelerating the decomposition of H_2O_2 to form $OOH^{\bullet}$ radicals. Meanwhile, ≡Fe(III) is photoreduced to ≡Fe(II) under irradiation by UVA light. Then, ≡Fe(II) promotes the decomposition of H_2O_2 to highly oxidative $OH^{\bullet}$ radicals whereas ≡Fe(II) is oxidized by H_2O_2 to ≡Fe(III). Furthermore, the $OOH^{\bullet}$ and $OH^{\bullet}$ radicals attack RB5 adsorbed onto the surface of the catalyst (≡Fe(III)···Azo-dye) to yield intermediates. Finally, some of the intermediates on ≡Fe(III) redissolve into the bulk solution, and the rest are mineralized to CO_2 and H_2O.

4. Conclusions

This investigation proposes a novel catalyst of the photoassisted Fenton degradation of azo-dye RB5. The catalyst greatly promotes not only the decolorization but also the mineralization of RB5 at neutral pH. Furthermore, this catalyst is much cheaper than Nafion-based catalysts. The main parameters that affect the degradation of RB5 have been detailed. A simple mechanism by which the heterogeneous catalyst discolors and mineralizes RB5

is presented, based on experimental results. This technique can be employed as the basis of a cost-effective method Fenton-type degradation of a pollutant, without the end-of-pipe discharge of iron sludge into the environment.

Acknowledgements

The authors thank the Ministry of Economic Affairs of the Republic of China and National Science Council of the Republic of China for financially supporting this research under Contract No. TDPA:91-EC-17-A-05-S1-0014 and NSC93-2622-E-006-026-CC3.

References

[1] I. Arslan, I. Akmehmet Balciogglu, Dyes Pigments 43 (1999) 95–108.
[2] S.F. Kang, C.H. Liao, M.C. Chen, Chemosphere 46 (2002) 923–928.
[3] J.A. Theruvathu, C.T. Aravindakumar, R. Flyunt, J.V. Sonntag, C.V. Sonntag, J. Am. Chem. Soc. 123 (2001) 9007–9014.
[4] B.D. Lee, M. Hosomi, Water Res. 35 (2001) 2314–2319.
[5] J.J. Pignatello, Environ. Sci. Technol. 26 (1992) 944–951.
[6] G. Ruppert, R. Bauer, G. Heisler, S. Novalic, Chemosphere 27 (1993) 1339–1347.
[7] J. Kiwi, C. Pulgarin, P. Peringer, Appl. Catal. B: Environ. 3 (1994) 335–350.
[8] M.E. Balmer, B. Sulzberger, Environ. Sci. Technol. 33 (1999) 2418–2424.
[9] K. Wu, Y. Xie, J. Zhao, H. Hidaka, J. Mol. Catal. A: Chem. 144 (1999) 77–84.
[10] P.L. Huston, J.J. Pignatello, Environ. Sci. Technol. 30 (1996) 3457–3463.
[11] W. Gernjk, T. Krutzler, A. Glaser, S. Malato, J. Caceres, R. Bauer, A.R. Fernandez-Alba, Chemosphere 50 (2003) 71–78.
[12] Y.H. Huang, G.H. Huang, S.S. Chou, H.S. You, S.H. Perng, US Patent 6,143,182 (2000).
[13] S. Chou, C. Huang, Y.H. Huang, Chemosphere 39 (1999) 1997–2006.
[14] S. Chou, C. Huang, Y.H. Huang, Environ. Sci. Technol. 35 (2001) 1247–1250.
[15] J. Fernandez, J. Bandara, A. Lopez, P. Alberz, J. Kiwi, Chem. Commun. (1998) 1493–1494.
[16] J. Fernandez, J. Bandara, A. Lopez, Ph. Buffar, J. Kiwi, Langmuir 15 (1999) 185–192.
[17] J. Fernandez, M.R. Djananjeyan, J. Kiwi, Y. Senuma, J. Hilborn, J. Phys. Chem. 104 (2000) 5298–5301.
[18] M.R. Djananjeyan, J. Kiwi, P. Albers, O. Enea, Helv. Chim. Acta 84 (2001) 3433–3455.
[19] A. Bozzi, T. Yuranova, J. Mielczarski, A. Lopez, J. Kiwi, Chem. Commun. (2002) 2202–2203.
[20] J. Feng, X. Hu, P.L. Yue, H.Y. Zhu, G.Q. Lu, Ind. Eng. Chem. Res. 42 (2003) 2058–2066.
[21] J. Feng, X. Hu, P.L. Yue, H.Y. Zhu, G.Q. Lu, Chem. Eng. Sci. 58 (2003) 679–685.
[22] G.L. Puma, P.L. Yue, Proceedings of the Sixth International Conference on Advanced Oxidation Technologies for Water and Air Remediation, London, Ont., Canada, June 26–30, 2000, p. 105.
[23] C.L. Wilson, N.W. Hinman, W.J. Cooper, C.F. Brown, Environ. Sci. Technol. 34 (2000) 2655–2662.
[24] Y.H. Huang, G.H. Hwang, S. Chou, H.S. You, S.H. Perng, Holland Patent 1009661, ITRI/Union Chemical Laboratories, Taiwan (2000).
[25] S. Chou, C. Huang, Chemosphere 38 (1999) 2719–2731.
[26] W. Stumm, Chemistry of the Solid–Water Interface, Wiley/Interscience, New York, 1992.
[27] S. Roland, S. Ingbert, S. Hans-Henning, Water Res. 31 (1997) 1371–1378.
[28] M. Neamtu, I. Siminiceanu, A. Kettrup, Dyes Pigments 53 (2002) 93–99.
[29] M. Koch, A. Yediler, D. Lienert, G. Insel, A. Kettrup, Chemosphere 46 (2002) 109–113.
[30] M. Neamtu, C. Catrinescu, A. Kettrup, Appl. Catal. B: Environ. 51 (1) (2004) 149–157.
[31] P. Mazellier, B. Sulzberger, Environ. Sci. Technol. 35 (2001) 3314–3320.
[32] J. He, W. Ma, J. He, J. Zhao, J.C. Yu, Appl. Catal. B: Environ. 39 (2002) 211–220.
[33] C. Walling, S.I. Kato, J. Am. Chem. Soc. 93 (1971) 4275–4281.
[34] S.S. Chou, C.P. Huang, Appl. Catal. A: Gen. 185 (1999) 237–245.
[35] C.L. Hsueh, Y.H. Huang, C.C. Wang, C.Y. Chen, Chemosphere 58 (2005) 1409–1414.